PAPER

Check for updates

Effect of the protein environment on the excited state phenomena in a bacteriophytochrome†

Pradipta Dey, [ID] Supriyo Santra [ID] and Debashree Ghosh [ID] *

The excited state processes of a bacteriophytochrome are studied using high-level multireference methods. The various non-radiative channels of deactivation are identified for the chromophore. The effects of the protein environment and substituents are elucidated for these excited state processes. It is observed that while the excited states are completely delocalized in the Franck–Condon (FC) region, they acquire significant charge transfer character near the conical intersections. Earlier studies have emphasized the delocalized nature of the excited states in the FC region, which leads to absorption spectra with minimal Stokes shift [Rumyantsev *et al.*, *Sci. Rep.*, 2015, **5**, 18348]. The effect of the protein environment on the vertical excitation energies was minimal, while that on the conical intersection (CI) energetics was significant. This may lead one to believe that it is charge transfer driven. However, energy decomposition analysis shows that it is the effect of the dispersion of nearby residues and the steric effect on the rings and substituents that lead to the large effect of proteins on the energetics of the CIs.

1 Introduction

Phytochromes are photoreceptors found in cyanobacteria,[1] fungi,[2] and non-photosynthetic bacteria in addition to plants.[3] There are many examples such as biliverdin (BV; non-photosynthetic bacteria),[4–6] phycocyanobilin (PCB; photosynthetic cyanobacteria),[1] phytochromobilin (oat phytochrome),[7] *etc.* and they differ slightly in their chromophore structure and substituents. However, the core structure of the chromophore remains the same, consisting of four pyrrole rings connected by methine bridges. They regulate a wide range of physiological responses ranging from phototaxis in bacteria to seed germination, growth, organelle development, *etc.*, in plants.[8,9] They function as temperature sensors and are mainly involved in the photoactivity of plants and their growth. In bacteria and several aquatic species, they are involved in the absorption of light at low intensities.[10,11]

As mentioned above, the chromophore of the phytochromes consists of a tetrapyrrole structure that has similarities to chlorophyll. The four pyrrole rings are denoted as A, B, C, and D rings, starting from the pyrrole that is connected to the cysteine residue (shown in Fig. 1). The pyrroles in phytochromes are linearly arranged, while in chlorophyll they are circularly organized, and this shifts the spectral maxima quite significantly.[12,13] Phytochromes show photoactivity in the red and far red regions of the visible spectra. They have two main

photo-interconvertible forms, called Pr and Pfr, denoting red (700 nm) and far red (754 nm) absorbances, respectively (shown in Fig. 1).[14,15]

Photoisomerization across double bonds, *i.e.*, *cis–trans* isomerization initiated by photoactivation, is a common process in several biological species, such as rhodopsins,[16] carotenoids,[17] *etc.* In phytochromes, several such photoisomerization sites are present across all methine bridges. However, biologically observed isomerization occurs only at the last methine bridge (between the C and D rings) to form the Pfr structure.[4] It is, therefore, crucial to understand the cause behind this process and its specificity. Furthermore, it is known that despite efficient absorption of light by the phytochromes, they are non-fluorescent.[18,19] Therefore, ultrafast nonradiative decay channels are expected.

The crystal structures of the bacterial[4–6] and cyanobacterial[1] phytochromes show that the A-ring of the chromophore binds to the protein *via* a thioether bond of the cysteine residue, while the D ring is free at the far end. The orientation of the adjacent pyrrole rings is *Z*, *Z*, *Z* with respect to the double bond and *syn*, *syn*, *anti* with respect to the single bond of the methine bridge. Due to this reason, the Pr form of the chromophore (which is the resting state) is also denoted as *ZZZssa*. The protein interacts with the chromophore in such a way that allows only the $C_{15}=C_{16}$ bond isomerization.[9] Therefore, upon excitation by red light, when the photoconversion occurs and the Pfr structure is formed, the configuration changes to *ZZEssa*. The photocycle of conversion between these forms is shown in detail in Fig. 1.[18]

NMR,[20] time-resolved mid-IR,[21,22] resonance Raman (RR),[23–25] and time-resolved femtosecond Raman spectral studies[26] have

School of Chemical Sciences, Indian Association for the Cultivation of Science, Jadavpur, Kolkata 700032, India. E-mail: pcdg@iacs.res.in

† Electronic supplementary information (ESI) available. See DOI: https://doi.org/10.1039/d4cp02112f

This journal is © the Owner Societies 2024

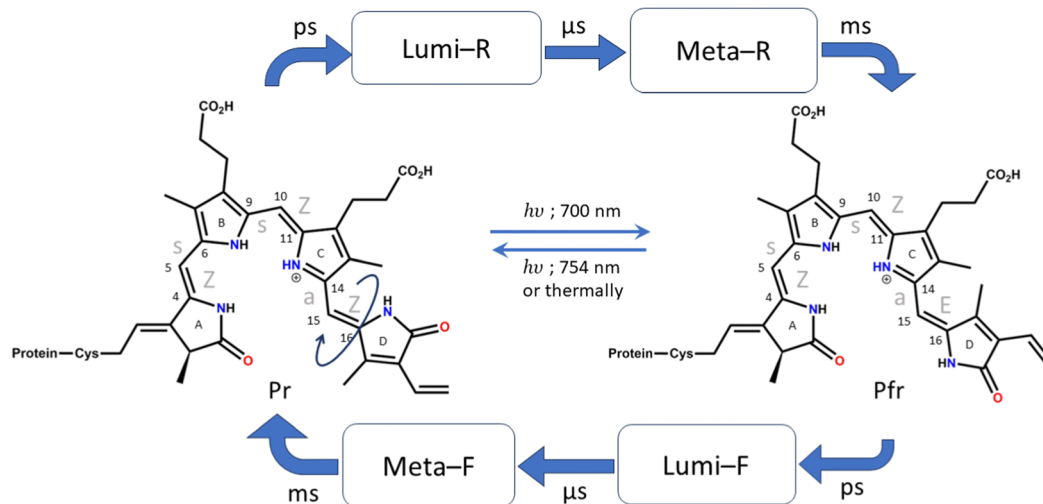*Phys. Chem. Chem. Phys.*, 2024, **26**, 20875–20882 | 20875

Fig. 1 Photocycle of Pr to Pfr photoconversion and Pfr to Pr photoconversion. The names of the intermediates are shown. Typical timescales are given above the arrows for the formation of those intermediates. The chromophore and conformation of the Pr and Pfr forms are shown, and the atoms in the methine bridge are numbered.

elucidated the first intermediate Lumi-R structure as the primary photoproduct formed during Pr to Pfr photoconversion. The Lumi-R formation takes around 30 ps.[26]

The protonation state of the chromophore has been studied theoretically[27,28] and experimentally[29–31] and the fully protonated structure is expected to be in the Pr form. However, some studies have also proposed protein-aided proton release and uptake mechanisms during photoconversion.[32]

There have been several theoretical studies to characterize the primary photoconversion step. The absorption spectra have been studied, and the effect of different isomers on the spectral intensities has been elucidated.[33–35] Durbeej and co-workers have observed isomerization about the C_9–C_{10} and C_{10}–C_{11} bonds using the TDDFT method (rotation around the central methine bridge).[36,37] Since this is not a biologically relevant isomerization step, other levels of theory have been employed to understand the C_{15}–C_{16} isomerization. However, due to the steep computational cost of multireference methods, either a truncated model has been used or semi-empirical methods have been resorted to. From a truncated model consisting of only two pyrrole rings, the effects of clockwise and anti-clockwise rotations and substitution have been studied.[38] Here, it has been observed that one bond flip becomes a preferred mechanism over hula twist upon carbonyl substitution. Minimal effects of alkyl group substitution were also observed. On the other hand, the study that considered the full chromophore while resorting to semi-empirical methods (OM2/MRCI) shows that isomerization across the C_9–C_{10} and C_{10}–C_{11} bonds becomes predominant.[28] This result was similar to that obtained from earlier TDDFT observations.[36,37]

Garavelli and co-workers[39] have done CIS/CASPT2 calculations and observed C_9–C_{10}/C_{10}–C_{11} and C_{15}–C_{16} bond isomerization pathways. Slavov et al.[40] have shown the tendency of the D ring of the chromophore to undergo counterclockwise rotation through QM/MM computations. QM/MM dynamics of the dimer protein were used to observe the evolution of the C_{15}–C_{16}

bond rotation, and they observed a similar counterclockwise rotation[41] to that reported in a previous study. Mennucci and co-workers have shown the effect of a protein on the dynamics of photoisomerization using the FOMO-CASCI method.[42] They have observed C_{15}–C_{16} isomerization in the protein environment. From all these observations, it is clear that multireference methods are crucial to appropriately describe the relative energetics of different bond rotations in the phytochrome.

In this study, we have investigated the initial step of photoisomerization of the BV chromophore in the gas phase and used multireference methods with sufficient active space to appropriately describe the potential energy surface (PES). We have worked with the fully protonated chromophore in the Pr form. The effect of a protein on the PES is also studied at both CASPT2 and TDDFT levels of theory to ascertain the most important interactions that modulate the energetics of the pathways.

2 Computational details

An isolated BV chromophore was taken from a PDB ID-2O9C,[5] and the fully protonated form of the chromophore was used. Fig. 2a shows the protein and the chromophore structure. The unsubstituted (alkyl groups are removed) small chromophore is shown in Fig. 2b. This small chromophore form is used for the most detailed study to calculate the PES and nonradiative decay pathways. The ground state geometry is optimized at the B3LYP/6-31G(d) level of theory. VEEs for the Franck–Condon (FC) region are calculated at various levels of theory – TDDFT[43,44] with B3LYP and CAM-B3LYP functionals and 6-31G(d) and 6-311++G(d,p) basis sets, EOM-CCSD/6-31G(d),[45] CASSCF[46] and CASPT2[47] with (6o,6e) active space and the 6-31G(d) basis set. State-specific CASPT2 calculations with a level shift of 0.25 a.u. are used to avoid the problem of intruder states.

CASSCF with (6o,6e) and TDDFT have been used to calculate the stationary points of the excited state surface, including the S_1-Min and conical intersections. The minimum energy
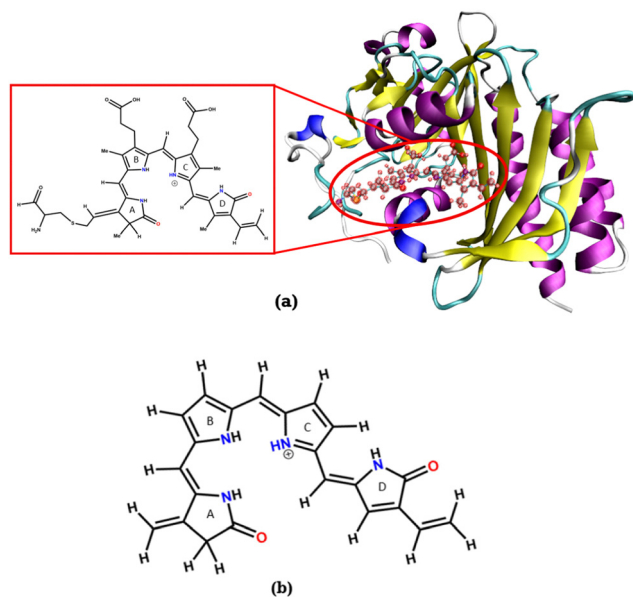
Fig. 2 (a) Structure of the bacteriophytochrome BV in a protein, the large chromophore considered for the chromophore in protein calculations (shown in the inset) and (b) the chromophore without the substituents (Chr-sm).

pathways (MEPs) between FC, S_1-Min, and the CIs are constructed to study the non-radiative decay mechanism. Then, single-point calculations were done on each geometry at CASPT2/6-31G(d) level of theory to create the surface.

To study the fate of the molecule after reaching the CIs, the 3D surfaces around the CIs are created using four topological parameters of the system,[48] namely

$$\sigma_x = \frac{S^{0i} \cdot \hat{x}}{d_{gh}}$$

$$\sigma_y = \frac{S^{0i} \cdot \hat{y}}{d_{gh}}$$

$$\Delta_{gh} = \frac{g^2 - h^2}{d_{gh}^2}$$

$$d_{gh} = \sqrt{(g^2 + h^2)}$$

where S^{0i} is the gradient sum vector with i representing the state with which the ground state has a CI (here i is 1) and $\hat{x}$ and $\hat{y}$ are the unit vectors based on the Schmidt-orthogonalised energy gradient difference vector (g^{0i}) and the derivative coupling vector (h^{0i}), which are given as

$$\hat{x} = \frac{g^{0i}}{\|g^{0i}\|}$$

$$\hat{y} = \frac{h^{0i}}{\|h^{0i}\|}$$

The parameters σ_x and σ_y give the tilt of the cone and d_{gh} and Δ_{gh} denote the pitch and divergence of the cone. These

parameters help to understand the fate of the molecule after reaching the CI.

The SA-CASSCF and state-specific CASPT2 calculations were done using Molpro-2015 software.[49] The CASPT2/MM calculations were done using Molpro-2024 software.[50] All TDDFT single-point calculations, excited state optimizations, EOM-CCSD excitation energies and the TDDFT/MM calculations were done using Q-Chem 5.1 software.[51]

The configurations around the methine bridges are shown by the dihedral angles denoted as – τ_{A-B}, τ_{B-A} between A and B rings, τ_{B-C}, τ_{C-B} between B and C rings, and τ_{C-D}, τ_{D-C} between C and D rings. Dihedral $N_A-C_4=C_5-C_6$, *i.e.*, the N of the A ring and the methine bridge C atoms between A and B rings, is referred to as τ_{A-B}, while the same for the N of the B ring is referred to as τ_{B-A} and so on.

For the chromophore in protein calculations, the Amber force field (ff14SB)[52] was used and solvated in TIP3P water.[53] For the cysteine attached BV chromophore the parameters were generated using the parmchk2 program and ff14SB force field and Amber atom types. The solvated protein crystal structure was then optimized. With this optimized structure, excited state QM/MM calculations were performed with TDDFT and CASPT2 as the QM method and point charges of the Amber force field for protein residues. The TIP3P charges on nearby water molecules were also included in the excited state QM/MM calculations.

The FC and CI geometries of the gas phase were embedded in the protein. The gas phase (Chr-sm) geometries were first placed in the protein cavity by translation and rotation of these geometries with respect to the crystal structure of the protein and its cavity. The extra propionate and cysteine groups were added to Chr-sm and therefore a large chromophore structure was formed. The part of the chromophore denoted as Chr-sm was kept fixed and the propionate groups and the protein around it were relaxed at the MM level of theory. This protocol was followed for FC and CI geometries. Then QM/MM calculations were done to determine the effective energies of those optimized geometries in the protein environment. This protocol preserves the structure of the CI as obtained in the gas phase while studying the effect of the protein environment and substituents on the energetics of the excited state PES. However, as artifacts of this protocol it should be mentioned that the CIs in the protein will be approximate in nature.

3 Results and discussion

The B3LYP/6-31G(d) optimized structure of the ground state is given in the ESI† (S11) and also shown in Fig. 3. The optimized ground state geometry of the chromophore is somewhat out of plane with a dihedral angle of 16° between A and B rings, 10.50° between the B and C rings, and about 14° between the C and D rings.

3.1 Vertical excitation energy and absorption spectra

As noted in the earlier literature, there are significant differences in the absorption spectra of the phytochrome chromophore[14] and

This journal is © the Owner Societies 2024

Phys. Chem. Chem. Phys., 2024, **26**, 20875–20882 | **20877**

porphyrin.[54–57] In this work, since we are interested in the excited state processes at the lowest optically bright state, we target only two excited states in our calculations. Both these excited states are π–π^* in nature. However, it is only the first excited state S_1 that is optically bright. The S_2 state is mostly optically dark.

Table 1 shows the excitation energies of these states calculated using TDDFT (B3LYP and CAM-B3LYP), EOM-EE-CCSD, and CASPT2(6,6) with the 6-31G(d) basis set. The oscillator strengths are mentioned in brackets. The effect of the basis set is also checked at the TDDFT level with the 6-311++G(d,p) basis set. It shows very little effect of the basis set on the excitation energy (given in Table S1, ESI†). The reason for the low effect of the basis set can be understood from the orbitals involved in the excitations (also shown in Table 1). Since both the excitations are purely π and π^* in nature, it is unsurprising that the effect of the basis set is minimal.

The excitation is completely delocalized over the chromophore, with no charge transfer component. The Mulliken charge analysis done on different parts of the optimized Chrsm has a qualitative similarity to those of a recent study,[58] yet we did not observe any charge transfer as evident from the attachment detachment density analysis shown in ESI† (Fig. S4). This is the reason why the absorption spectra remain at the same position irrespective of mutations.[35,59] This is also the reason behind high oscillator strength and the ability of the phytochrome to absorb strongly in this red region. The orbitals involved in the (6o,6e) active space are given in Fig. S1 (ESI†). Since between the first two excitations, the only orbitals involved are the HOMO, HOMO−1, and LUMO, the (6o,6e) active space is adequate.[39] In ref. 39, several active spaces have been tested, and it was observed that the size of active space has very little effect on the nature and energy of the S_1 state.

3.2 Excited state potential energy surface

The optimized geometry for the S_1 minimum is given in Fig. S5 (ESI†). The S_1 minimum is near the ground state geometry. This is expected since there is no charge transfer component in the excited state, and therefore, the S_1 has a similar electron density to the ground state.
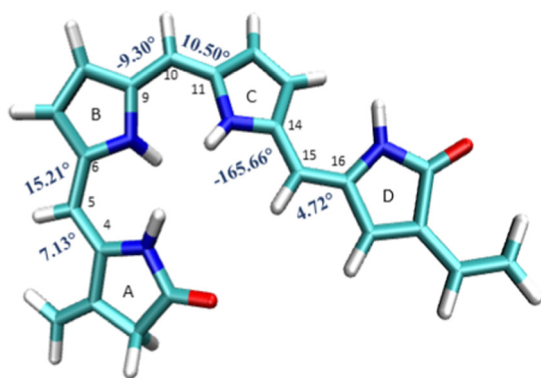

Fig. 3 Geometrical parameters of FC: (a) dihedral angles τ_{A-B}, τ_{B-A}, τ_{B-C}, τ_{C-B}, τ_{C-D} and τ_{D-C} (in degrees).

Two conical intersections could be obtained for the molecule between the S_1 and S_0 states (shown in Fig. 4a and b). CI_1 (Fig. 4a) consists of an anticlockwise rotation of the D-ring. CI_2 (Fig. 4b), on the other hand, has the rotation of the A and B rings, or it can be envisaged as a C and D ring rotation. Since the S_1 state is an excitation state delocalized over the chromophore, the CIs can be obtained by reducing the conjugation length. The rotation of the different rings out of the molecular plane leads to a reduction in the effective conjugation length and, therefore, causes the near degeneracy between the S_0 and S_1 states. It is also unsurprising that the CD ring rotation causes a greater reduction in the conjugation length and, therefore, leads to a lower energy or easier-to-access CI. The effective reduction in the conjugation can be noticed from the dihedral angles and bond lengths of the methine bridge C–C bond lengths (shown in Table 2). The dihedral angles at both the CIs show a complete perpendicular geometry between C–D or B–C rings, respectively (the values of dihedral angles are tabulated in Table S2, ESI†). The alternating double and single bonds in the methine bridges are also disturbed at those locations.
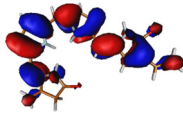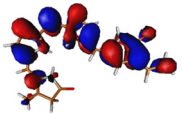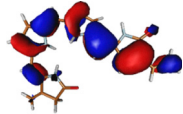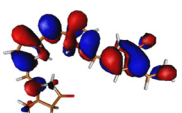
Fig. 5 shows the minimum energy pathways from the FC/S_1 minimum to the two CIs. At the CASPT2 level of theory, the CI_1 is much higher in energy than the S_1 state at the FC region (>8 kcal mol^{-1}), while an energy barrier of 2 kcal mol^{-1} is observed to reach C–D ring rotated CI_2. Therefore, the CI_2 is energetically easier to approach in the gas phase than CI_1. This gas phase observation is contrary to the observation of the Lumi-R structure in proteins, which is closer to the CI_1 structure, i.e., involves D ring rotation. Therefore, large effects of the protein environment are expected.

The orbitals involved in the S_1 excitation near the CI are shown in Fig. S6 in the ESI.† It shows large changes in electron density at these geometries. The CI_1 shows the charge transfer component from the B and C rings to the D ring. The CI_2 shows the charge transfer component from C and D rings to A and B rings.

We have calculated the parameters associated with the topology of the CIs and have re-created the linearly interpolated structure of the CIs. For the high energy CI_1, the tilt of the cone (Fig. 6a) is towards the positive of the $\vec{h}$ vector and negative of the $\vec{g}$ vector (the vectors are shown in Fig. S8, ESI†). This observation shows that there is an equal probability of the molecule undergoing photo-product formation and photoprotection (returning to the Franck–Condon region) for this CI. The $\vec{h}$ vector corresponds to out of plane bending motion of the C_{14}–C_{15} and C_{15}–C_{16} bonds. It also shows asymmetric stretching of C_9–C_{10} and C_{10}–C_{11} bonds. The photoproduct will form by the torsion of τ_{C-D} and τ_{D-C} dihedrals as it involves out-of-plane rotation.

The energetically accessible CI_2 describes simultaneous torsion of τ_{B-C} and τ_{C-B} dihedral angles. The topology of CI_2 (Fig. 6b) has a tilt towards the negative of the $\vec{g}$ vector and is symmetric about the $\vec{h}$ vector. This refers to a greater probability of the molecule undergoing photoprotection than forming a photoproduct. The $\vec{h}$ vector corresponds to the out of

20878 | *Phys. Chem. Chem. Phys.*, 2024, **26**, 20875–20882

This journal is © the Owner Societies 2024

Table 1 Singlet excited energies at different levels of theory using the 6-31G(d) basis set. The excitation values are in eV. The oscillator strengths are given in brackets

Excited state	B3LYP	CAM-B3LYP	EOM-EE-CCSD	CASPT2	Orbitals from	To
S_1	1.99 (0.95)	2.10 (1.04)	2.53 (1.33)	1.65 (1.45)		
S_2	2.48 (0.07)	3.25 (0.27)	3.63 (0.04)	2.26 (0.17)		

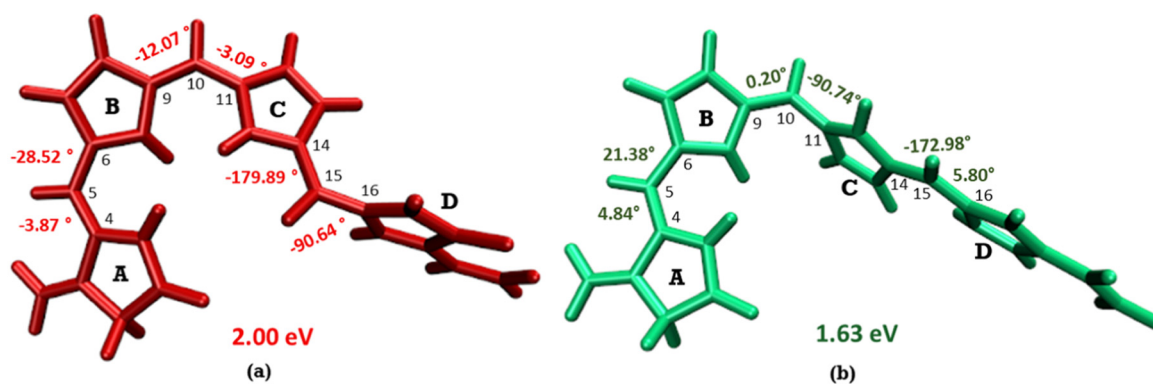**Fig. 4** (a) CI_1, D ring rotated CI and (b) CI_2, C−D ring rotated CI with their respective dihedral angle values.

plane motion of C_9–C_{10} bonds and C_{10}–C_{11} bonds (shown in Fig. S8, ESI†). From this information, it is inferred that if photoproduct formation occurs, it must involve the isomerization of the bridge connecting the B and C pyrrole rings.

3.3 Effect of substituents and the protein environment

To understand the effect of substituents on the excited state surface, the S_0 and S_1 energies were calculated with the large chromophore at the FC and CI geometries. The substituents and added atoms were relaxed for all these calculations. No large effects were observed in this case, proving that the substituents, especially the alkyl groups, do not alter the PES significantly.

To understand the effect of the protein environment, the chromophore with the protein was taken. The protein structure was relaxed while keeping the chromophore geometry fixed at the FC or CI geometries. With this geometry, further QM/MM computations were performed at the B3LYP/MM and CASPT2/MM levels of theory.

Table 2 Comparison of bond lengths at several geometries (in Å)

Geometry	C_4–C_5	C_5–C_6	C_9–C_{10}	C_{10}–C_{11}	C_{14}–C_{15}	C_{15}–C_{16}
FC	1.37	1.42	1.40	1.39	1.42	1.37
S_1-Min	1.39	1.40	1.36	1.44	1.43	1.37
CI_1	1.33	1.46	1.42	1.36	1.34	1.45
CI_2	1.35	1.44	1.36	1.46	1.40	1.36

Table 3 shows the energy of the FC, CI_1 and CI_2 of the gas phase and in the protein system calculated at the TDDFT/MM level of theory. It is observed that while in the gas phase, CI_2, *i.e.*, rotation of both C and D rings (across the central methine bridge), is lower in energy, the protein environment destabilizes this CI. On the other hand, the CI_1, *i.e.*, rotation of only the D ring, is significantly stabilized in the protein environment. This leads to the facile D ring rotation in the protein en route to the Lumi-R structure. A similar effect is seen for CASPT2, where due to the extra stability of the protein environment, the CI_1 g.s. is stabilized by 4.38 kcal mol^{-1} (0.19 eV), while CI_2 g.s. is destabilized by 44.04 kcal mol^{-1}. Steric effects and lack of favourable dispersion interactions primarily drive the large de-stabilization of CI_2.

Here, it should also be noted that the embedding of gas phase geometries in the protein is an approximation due to which the exact geometry of the CIs gets significantly affected as noticed from the somewhat lack of degeneracy between the ground and excited states at the gas phase CI geometries with the protein environment.

To decompose the effect of the nearby residues and ascertain the main cause of the extra stabilization of CI_1 in the protein, EDA analysis is performed with HIS290, HIS260, TYR263, and PHE203. The details of the EDA analysis are included in Table S3 in the ESI.† Quite surprisingly, it was noticed that TYR263 and PHE203 showed significant stabilization effects on the CI_1 structure, and this was mainly due to the dispersion interaction between the D ring and the
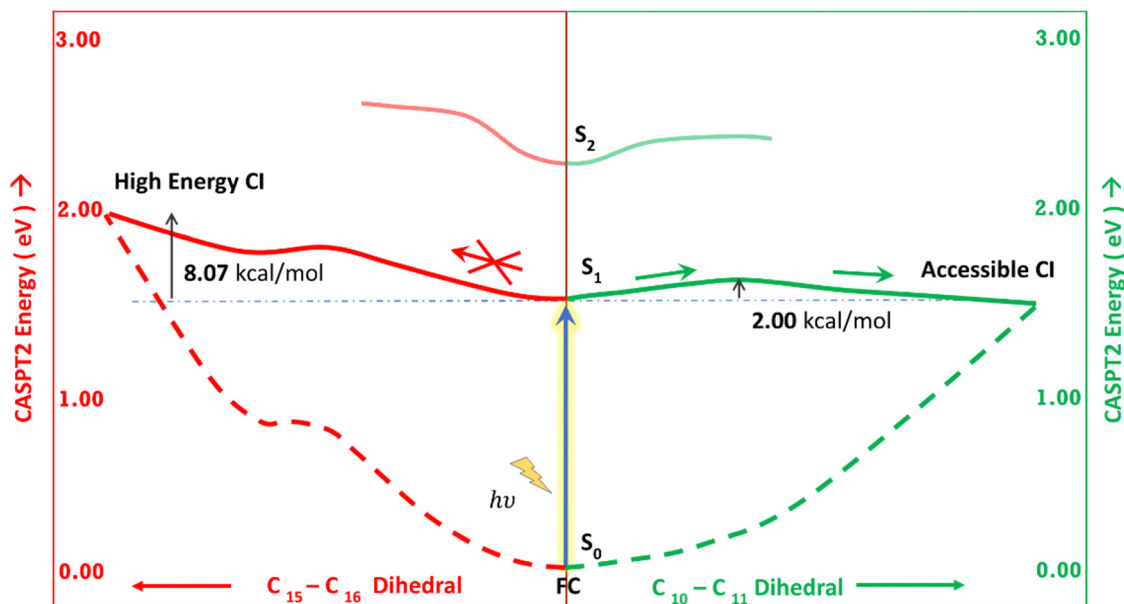
This journal is © the Owner Societies 2024

Phys. Chem. Chem. Phys., 2024, **26**, 20875–20882 | **20879**

Fig. 5 Schematic representation of the two MEPs. The left side refers to the pathway from FC to CI_1 (red). The right side refers to the pathway from FC to CI_2 (green). MEPs are calculated at the CASPT2/6-31g(d) level of theory.
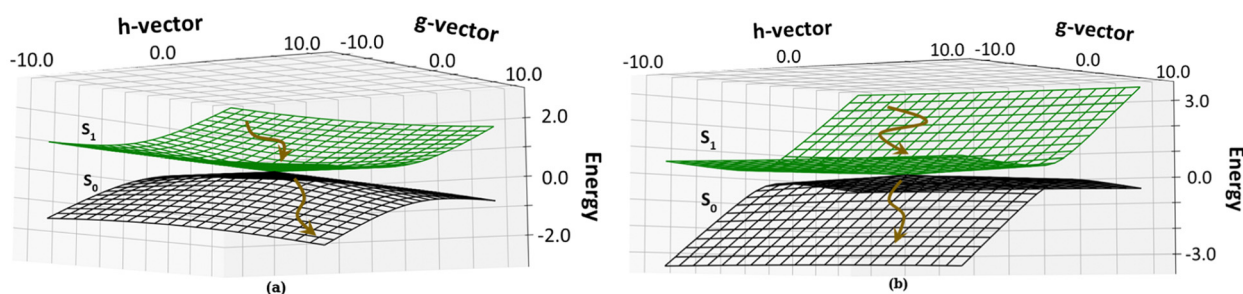

Fig. 6 Topology around the Cis: (a) CI_1, D ring rotated CI and (b) CI_2, C–D ring rotated CI. The deactivation of the chromophore from the S_1 state to the S_0 state is shown by brown arrows.

Table 3 S_1 state energy (in eV) with respect to FC (S_0) for Chr-min, the large chromophore and the chromophore in the protein medium at the TD-B3LYP/6-31G(d) level of theory

System	CI_1	FC	CI_2
Chr-min	2.04	1.99	1.48
Large chromophore	1.92	1.91	1.67
Chromophore in protein	1.27	1.62	1.92

amino acids. In CI_2, both these interactions were largely absent due to large distances and mismatch of ring faces. Furthermore, it is noteworthy that HIS290, which is near the D ring, does not show much differential effect on the stability of the CIs. This is true even though the excited states in the CIs show a significant charge transfer component. The reason could be the relatively large distance of the HIS290 from the ring itself. On the other hand, HIS260, which remains stacked in FC geometry between the B and C rings, offers preferential stability to the CI_1. This is because the B and C rings remain unchanged in the CI_1 and FC geometry. On the other hand,

in CI_2 due to rotation around the central methine bridge, this stacking interaction is largely diminished, thereby preferentially destabilizing the CI_2 conformer. The tethering effect of the alkyl carboxylic acid substituents could also result in the destabilization of the CI_2 geometry. Essentially, the tethers retain the B and C rings in the original FC geometry and deter rotation around the methine bridge between these rings.

To surmise the effect of substituents, carboxylic acid groups and the protein environment cause the CI_1 to be preferred. The modulation by these factors is mainly driven by steric and dispersion interactions rather than specific H-bond or electrostatic interactions. This observation corroborates with the earlier study conducted by Durbeej and co-workers.[60]

4 Conclusion

In summary, we have studied the bacteriophytochrome chromophore's excited state potential energy surface using high-level multireference methods. We have noticed that the excited states are delocalized and do not involve a charge transfer

20880 | *Phys. Chem. Chem. Phys.*, 2024, **26**, 20875–20882

This journal is © the Owner Societies 2024

component. The lowest excited state is optically bright, characterized by high oscillator strength (absorption coefficient). Two low-energy conical intersections between the S_1 and ground states are found. The CIs involve rotation across methine bridges – either the central methine bridge or the one between the C and D rings. While in the gas phase, the CI along central methine bridge rotation is lower in energy, in the protein environment, this trend is reversed. This observation also proves the reason behind the varying results obtained in different theoretical studies.

Furthermore, the origin of a specific protein interaction that leads to preferential D ring rotation is ascertained. It is observed that the dispersion and steric interactions in proteins play a crucial role.

Author contributions

D. G. formulated the problem and computational approaches. P. D. and S. S. performed the calculations. D. G. and S. S. wrote the manuscript.

Data availability

All geometries (coordinates) and software versions used have been included/mentioned in the ESI† and main manuscript. No other data are required to reproduce the study.

Conflicts of interest

There are no conflicts to declare.

Acknowledgements

Notes and references

1 L.-O. Essen, J. Mailliet and J. Hughes, *Proc. Natl. Acad. Sci. U. S. A.*, 2008, **105**, 14709–14714.
2 A. C. Froehlich, B. Noh, R. D. Vierstra, J. Loros and J. C. Dunlap, *Eukaryotic Cell*, 2005, **4**, 2140–2152.
3 P. H. Quail, M. T. Boylan, B. M. Parks, T. W. Short, Y. Xu and D. Wagner, *Science*, 1995, **268**, 675–680.
4 J. R. Wagner, J. S. Brunzelle, K. T. Forest and R. D. Vierstra, *Nature*, 2005, **438**, 325–331.
5 J. R. Wagner, J. Zhang, J. S. Brunzelle, R. D. Vierstra and K. T. Forest, *J. Biol. Chem.*, 2007, **282**, 12298–12309.
6 X. Yang, E. A. Stojković, J. Kuk and K. Moffat, *Proc. Natl. Acad. Sci. U. S. A.*, 2007, **104**, 12571–12576.
7 M. J. Terry, M. T. McDowell and J. C. Lagarias, *J. Biol. Chem.*, 1995, **270**, 11111–11118.

8 N. C. Rockwell, Y.-S. Su and J. C. Lagarias, *Annu. Rev. Plant Biol.*, 2006, **57**, 837–858.
9 N. C. Rockwell and J. C. Lagarias, *Plant Cell*, 2006, **18**, 4–14.
10 J. Mach, *Phytochromes in Diatoms: Sensing Far-Red Light in the Deep Blue Sea*, 2016.
11 M. Legris, Y. Ç. Ince and C. Fankhauser, *Nat. Commun.*, 2019, **10**, 5219.
12 C. French, J. Brown and M. Lawrence, *Plant Physiol.*, 1972, **49**, 421–429.
13 G. Cinque, R. Croce and R. Bassi, *Photosynth. Res.*, 2000, **64**, 233–242.
14 R. Tasler, T. Moises and N. Frankenberg-Dinkel, *FEBS J.*, 2005, **272**, 1927–1936.
15 E. S. Burgie, J. Zhang and R. D. Vierstra, *Structure*, 2016, **24**, 448–457.
16 J. von Lintig, P. D. Kiser, M. Golczak and K. Palczewski, *Trends Biochem. Sci.*, 2010, **35**, 400–410.
17 H.-E. Khoo, K. N. Prasad, K.-W. Kong, Y. Jiang and A. Ismail, *Molecules*, 2011, **16**, 1710–1738.
18 D. Buhrke, F. Velazquez Escobar, L. Sauthof, S. Wilkening, N. Herder, N. N. Tavraz, M. Willoweit, A. Keidel, T. Utesch and M.-A. Mroginski, *et al.*, *Sci. Rep.*, 2016, **6**, 28444.
19 K. A. Rumyantsev, D. M. Shcherbakova, N. I. Zakharova, A. V. Emelyanov, K. K. Turoverov and V. V. Verkhusha, *Sci. Rep.*, 2016, **5**, 18348.
20 T. Rohmer, C. Lang, J. Hughes, L.-O. Essen, W. Gärtner and J. Matysik, *Proc. Natl. Acad. Sci. U. S. A.*, 2008, **105**, 15229–15234.
21 J. J. van Thor, K. L. Ronayne and M. Towrie, *J. Am. Chem. Soc.*, 2007, **129**, 126–132.
22 C. Schumann, R. Groß, N. Michael, T. Lamparter and R. Diller, *ChemPhysChem*, 2007, **8**, 1657–1663.
23 F. Andel, J. C. Lagarias and R. A. Mathies, *Biochemistry*, 1996, **35**, 15997–16008.
24 C. Kneip, P. Hildebrandt, W. Schlamann, S. E. Braslavsky, F. Mark and K. Schaffner, *Biochemistry*, 1999, **38**, 15185–15192.
25 F. Andel, J. T. Murphy, J. A. Haas, M. T. McDowell, I. van der Hoef, J. Lugtenburg, J. C. Lagarias and R. A. Mathies, *Biochemistry*, 2000, **39**, 2667–2676.
26 J. Dasgupta, R. R. Frontiera, K. C. Taylor, J. C. Lagarias and R. A. Mathies, *Proc. Natl. Acad. Sci. U. S. A.*, 2009, **106**, 1784–1789.
27 V. Modi, S. Donnini, G. Groenhof and D. Morozov, *J. Phys. Chem. B*, 2019, **123**, 2325–2334.
28 H. Huang, C. Xu, K. Lin, J. Peng, F. L. Gu and Z. Lan, *Chin. Chem. Lett.*, 2023, **34**, 107850.
29 T. Rohmer, H. Strauss, J. Hughes, H. de Groot, W. Gaertner, P. Schmieder and J. Matysik, *J. Phys. Chem. B*, 2006, **110**, 20580–20585.
30 D. Von Stetten, M. Günther, P. Scheerer, D. H. Murgida, M. A. Mroginski, N. Krauß, T. Lamparter, J. Zhang, D. M. Anstrom and R. D. Vierstra, *et al.*, *Angew. Chem., Int. Ed.*, 2008, **47**, 4753–4755.
31 J. A. Rumfeldt, H. Takala, A. Liukkonen and J. A. Ihalainen, *Photochem. Photobiol.*, 2019, **95**, 969–979.

This journal is © the Owner Societies 2024

Phys. Chem. Chem. Phys., 2024, **26**, 20875–20882 | **20881**

32 J. J. van Thor, B. Borucki, W. Crielaard, H. Otto, T. Lamparter, J. Hughes, K. J. Hellingwerf and M. P. Heyn, *Biochemistry*, 2001, **40**, 11460–11471.

33 R. A. Matute, R. Contreras, G. Pérez-Hernández and L. González, *J. Phys. Chem. B*, 2008, **112**, 16253–16256.

34 R. A. Matute, R. Contreras and L. González, *J. Phys. Chem. Lett.*, 2010, **1**, 796–801.

35 S. Santra, R. N. Manna, S. Chakrabarty and D. Ghosh, *J. Phys. Chem. B*, 2024, **128**, 3614–3620.

36 B. Durbeej, *Phys. Chem. Chem. Phys.*, 2009, **11**, 1354–1361.

37 A. Strambi and B. Durbeej, *Photochem. Photobiol. Sci.*, 2011, **10**, 569–579.

38 A. G. Rao and I. Schapiro, *Phys. Chem. Chem. Phys.*, 2022, **24**, 29393–29405.

39 P. Altoe, T. Climent, G. C. De Fusco, M. Stenta, A. Bottoni, L. Serrano-Andrés, M. Merchán, G. Orlandi and M. Garavelli, *J. Phys. Chem. B*, 2009, **113**, 15067–15073.

40 C. Slavov, T. Fischer, A. Barnoy, H. Shin, A. G. Rao, C. Wiebeler, X. Zeng, Y. Sun, Q. Xu and A. Gutt, *et al.*, *Proc. Natl. Acad. Sci. U. S. A.*, 2020, **117**, 16356–16362.

41 D. Morozov, V. Modi, V. Mironov and G. Groenhof, *J. Phys. Chem. Lett.*, 2022, **13**, 4538–4542.

42 G. Salvadori, V. Macaluso, G. Pellicci, L. Cupellini, G. Granucci and B. Mennucci, *Nat. Commun.*, 2022, **13**, 6838.

43 P. Hohenberg and W. Kohn, *Phys. Rev.*, 1964, **136**, B864–B871.

44 E. Runge and E. K. U. Gross, *Phys. Rev. Lett.*, 1984, **52**, 997–1000.

45 J. F. Stanton and R. J. Bartlett, *J. Chem. Phys.*, 1993, **98**, 7029–7039.

46 B. O. Roos, Ab Initio Methods in Quantum Chemistry Part 2, *Adv. Chem. Phys.*, 1987, **69**, 399–445.

47 J. Finley, P.-Å. Malmqvist, B. O. Roos and L. Serrano-Andrés, *Chem. Phys. Lett.*, 1998, **288**, 299–306.

48 M. Barbatti, A. J. Aquino and H. Lischka, *J. Phys. Chem. A*, 2005, **109**, 5168–5175.

49 H. Werner, P. Knowles, G. Knizia, F. Manby, M. Schütz, P. Celani, W. Györffy, D. Kats, T. Korona and R. Lindh, *et al.*, *MOLPRO, version 2015.1, a package of ab initio programs*, 2015.

50 H.-J. Werner, P. J. Knowles, F. R. Manby, J. A. Black, K. Doll, A. Heßelmann, D. Kats, A. Köhn, T. Korona and D. A. Kreplin, *et al.*, *J. Chem. Phys.*, 2020, **152**, 144107.

51 Y. Shao, Z. Gan, E. Epifanovsky, A. T. Gilbert, M. Wormit, J. Kussmann, A. W. Lange, A. Behn, J. Deng and X. Feng, *et al.*, *Mol. Phys.*, 2015, **113**, 184–215.

52 J. A. Maier, C. Martinez, K. Kasavajhala, L. Wickstrom, K. E. Hauser and C. Simmerling, *J. Chem. Theory Comput.*, 2015, **11**, 3696–3713.

53 P. Mark and L. Nilsson, *J. Phys. Chem. A*, 2001, **105**, 9954–9960.

54 M. Aydin and D. L. Akins, *Comput. Theor. Chem.*, 2018, **1132**, 12–22.

55 C. Weiss, *J. Mol. Spectrosc.*, 1971, **44**, 37–80.

56 J. Lin and D. Shi, *Appl. Phys. Rev.*, 2021, **8**, 011302.

57 M. Gouterman, *J. Mol. Spectrosc.*, 1961, **6**, 138–163.

58 E. Maximowitsch and T. Domratcheva, *ChemRxiv*, 2020, preprint, DOI: **10.26434/chemrxiv.12278780.v1**.

59 J. R. Wagner, J. Zhang, D. Von Stetten, M. Günther, D. H. Murgida, M. A. Mroginski, J. M. Walker, K. T. Forest, P. Hildebrandt and R. D. Vierstra, *J. Biol. Chem.*, 2008, **283**, 12212–12226.

60 O. Falklöf and B. Durbeej, *ChemPhysChem*, 2016, **17**, 954–957.